Iron–sulfur clusters/semiquinones in Complex I

Tomoko Ohnishi *

Johnson Research Foundation, Department of Biochemistry and Biophysics, and the University of Pennsylvania, Philadelphia, PA 19104, USA

Abstract

NADH-quinone [1] oxidoreductase (Complex I) isolated from bovine heart mitochondria was, until recently, the major source for the study of this most complicated energy transducing device in the mitochondrial respiratory chain. Complex I has been shown to contain 43 subunits and possesses a molecular mass of about 1 million. Recently, Complex I genes have been cloned and sequenced from several bacterial sources including *Escherichia coli*, *Paracoccus denitrificans*, *Rhodobacter capsulatus* and *Thermus thermophilus* HB-8. These enzymes are less complicated than the bovine enzyme, containing a core of 13 or 14 subunits homologous to the bovine heart Complex I. From this data, important clues concerning the subunit location of both the substrate binding site and intrinsic redox centers have been gleaned. Powerful molecular genetic approaches used in these bacterial systems can identify structure/function relationships concerning the redox components of Complex I. Site-directed mutants at the level of bacterial chromosomes and over-expression and purification of single subunits have allowed detailed analysis of the amino acid residues involved in ligand binding to several iron–sulfur clusters. Therefore, it has become possible to examine which subunits contain individual iron–sulfur clusters, their location within the enzyme and what their ligand residues are. The discovery of $g = 2.00$ EPR signals arising from two distinct species of semiquinone (SQ) in the activated bovine heart submitochondrial particles (SMP) is another line of recent progress. The intensity of semiquinone signals is sensitive to $\Delta\mu_H^+$ and is diminished by specific inhibitors of Complex I. To date, semiquinones similar to those reported for the bovine heart mitochondrial Complex I have not yet been discovered in the bacterial systems. This mini-review describes three aspects of the recent progress in the study of the redox components of Complex I: (A) the location of the substrate (NADH) binding site, flavin, and most of the iron–sulfur clusters, which have been identified in the hydrophilic electron entry domain of Complex I; (B) experimental evidence indicating that the cluster N2 is located in the amphipathic domain of Complex I, connecting the promontory and membrane parts. Very recent data is also presented suggesting that the cluster N2 may have a unique ligand structure with an atypical cluster-ligation sequence motif located in the NuoB (NQO6/PSST) subunit rather than in the long advocated NuoI (NQO9/TYKY) subunit. The latter subunit contains the most primordial sequence motif for two tetranuclear clusters; (C) the discovery of spin–spin interactions between cluster N2 and two distinct Complex I-associated species of semiquinone. Based on the splitting of the $g_{\parallel}$ signal of the cluster N2 and concomitant strong enhancement of the semiquinone spin relaxation, one semiquinone species was localized 8–11 Å from the cluster N2 within the inner membrane on the matrix side (N-side). Spin relaxation of

---

Abbreviations: EPR, electron paramagnetic resonance; FMN, flavin mononucleotide; Q, quinone; QH_2, quinol; SQ, semiquinone

* Corresponding author. Fax: +1-215-573-3748; E-mail: ohnishi@mail.med.upenn.edu

[1] Bovine heart Complex I contains only ubiquinone-10. Quinones in bacterial membranes differ depending on strains, for example, ubiquinone-10 in *R. capsulatus*; ubiquinone-8 in *P. denitrificans*; menaquinone-8 in *T. thermophilus*; both ubiquinone-8 and menaquinone-8 in aerobically grown *E. coli* cells (the ratio of UQ and MQ is controlled by oxygen tension). Therefore, in this mini-review, quinone (Q), quinol (QH_2), and semiquinone (SQ) were used for simplicity.

the other semiquinone species is much less enhanced, and thus it was proposed to have a longer distance from the cluster N2, perhaps located closer to the other side (P-side) surface of the membrane. A brief introduction of EPR technique was also described in Appendix A of this mini-review. © 1998 Elsevier Science B.V.

1. Introduction

NADH-quinone [1] oxidoreductase (more frequently called Complex I) located in the inner membrane of mitochondria catalyzes electron transfer from NADH to the quinone pool through a series of redox centers. Coupled to this process, $n = 4$–5 protons are vectorially translocated across the mitochondrial inner membrane as shown in the following equation:

$$NADH + Q + H^+ + n(H^+)_{in} \leftrightarrow NAD^+ \\ + QH_2 + n(H^+)_{out}$$
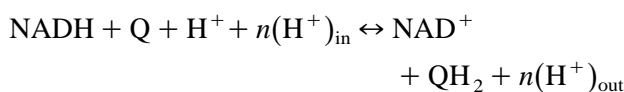
The detailed reaction mechanism is unknown, however, the intrinsic redox components involved in this reaction are one non-covalently bound FMN [1], at least six EPR detectable iron–sulfur clusters [2–4], and at least two distinct protein-bound species of quinone [5–7] (see Fig. 1). During the past decade, substantial progress has been made in the study of structural aspects of Complex I. The unusual L-shaped low resolution structural outline of Complex I was revealed by the electron microscopic analysis on the

2D-membrane crystal of *Neurospora crassa* and their isolated Complex I particles [8]. The complete primary sequence of 43 different subunits of highly purified bovine heart Complex I was determined [9–11] including seven mitochondrially encoded subunits [12]. The total molecular mass of the bovine heart Complex I approaches 1 million Da assuming that only one copy of each subunit is present in the complex.

Complex I has been found in plants, fungi, and in many bacteria (see individual chapters in this issues). The minimal functional unit of Complex I was found in bacteria which contain 13 to 14 conserved subunits [13–15] with or without auxiliary subunits encoded by unidentified reading frames (URFs). In *Escherichia coli* two of these subunits (C and D) are fused yielding 13 subunit enzyme [16]. The seven most hydrophobic bacterial subunits correspond to mitochondrially encoded subunits, whereas the remaining six or seven bacterial subunits correspond to homologous nuclear-encoded subunits in mitochondria. The complete primary sequences were deduced
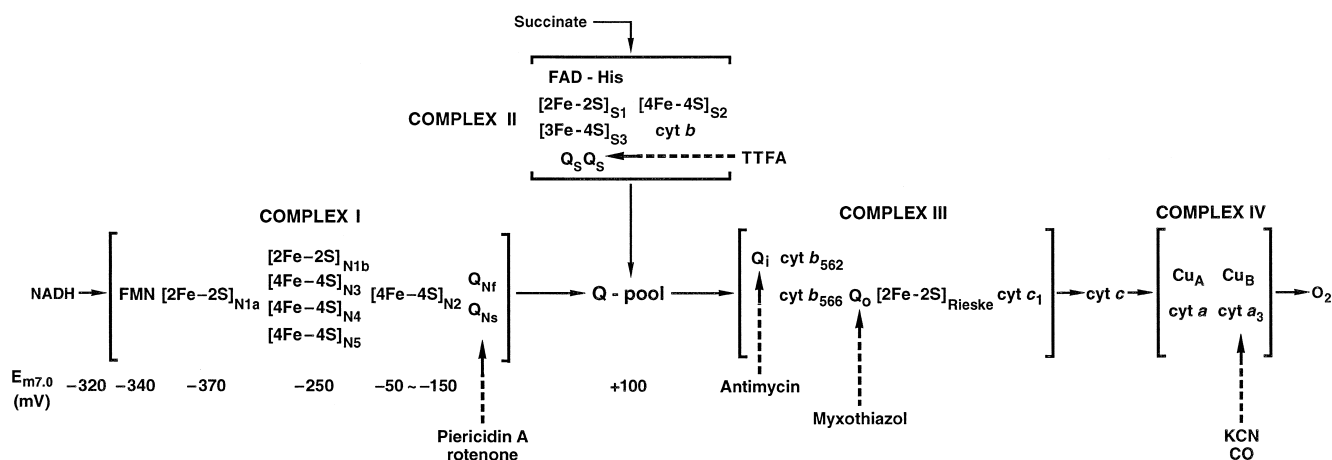

Fig. 1. Respiratory chain redox components in the inner membrane of bovine heart mitochondria are schematically shown. Iron–sulfur clusters in the NADH-UQ (Complex I) and succinate-UQ (Complex II) oxidoreductase segments are distinguished with suffixes Nx and Sx, respectively. Q_N, Q_S, and (Q_o and Q_i) denote specific UQ binding sites in Complex I, Complex II, and ubiquinol-cytochrome *c* oxidoreductase (Complex III) segment, respectively. Specific inhibitor binding sites are illustrated with arrows. Redox midpoint potentials at pH 7 ($E_{m7.0}$) of Complex I components are also shown.

from DNA sequences for *Paracoccus denitrificans* [14], *E. coli* [13] and *Thermus thermophilus* HB-8 [15] Complex I and partial sequence information has been published for *Rhodobacter capsulatus* [17,18]. *E. coli* and *T. thermophilus* HB-8 are known to contain two different NADH-quinone oxidoreductases designated as NDH-1 and NDH-2 [19,20]. The former is the counterpart of mitochondrial Complex I, while the latter is a single polypeptide containing FAD, no iron–sulfur clusters, and does not translocate protons vectorially across the membrane. Since the essential function of NDH-1 is the same as that of eukaryotic Complex I, NDH-1 is called Complex I in this review for the sake of simplicity.

A close structural and functional similarity between homologous 3D-structures of essential subunits of cytochrome *c* oxidase from *P. denitrificans* [21] and from bovine heart mitochondria [22,23] studied by high resolution X-ray structural analysis demonstrated the value of studying these complexes in the simpler bacterial systems. Since Complex I from bacteria and Complex I from bovine heart mitochondria are spectroscopically and functionally similar, containing equivalent redox components (as indicated by the fully conserved sequence motifs for flavin, NADH binding sites and ligands to iron–sulfur clusters), the bacterial Complex I can be studied as a simpler model of the mitochondrial Complex I.

EPR spectroscopic techniques combined with powerful genetic approaches, such as over-expression of individual subunits [20] and gene recombinant mutation at the level of the bacterial chromosome (Friedrich, this volume; Dupuis et al., this volume) have led to several discoveries. We have learned that all redox components with low midpoint potentials (E_m) are located within the promontory (peripheral) arm [24,25], while cluster N2 with the highest E_m value is located close to the interface between the membrane and the promontory arm. Recently, new experimental observations have emerged which strongly suggest that this cluster is located in NuoB (NQO6/PSST) subunit rather than in the long advocated NuoI (NQO9/TYKY) subunit. This notion will lead to future studies on a unique ligand structure of this functionally important iron–sulfur cluster in Complex I.

A discovery of the spin–spin interaction between two protein-associated species of semiquinone (i.e.,

SQ_{Nf} and SQ_{Ns}) and cluster N2 in the mitochondrial membrane, showed the existence of spatially separated and environmentally different quinone binding sites within the membrane part of Complex I. These SQ species are considered to play an important role in the proton/electron transfer mechanism, as proposed in another chapter of this issue together with Dutton and his colleagues.

Based on the recent progress using bacterial Complex I system, the structural aspects of the redox components of Complex I will be discussed in this chapter. Since EPR techniques are not commonly used in the bioenergetics field, and it is almost the sole spectroscopic technique so far used for Complex I studies, basic principles of this technique are briefly described in Appendix A for readers new to this field.

2. Nomenclature and composition of Complex I iron–sulfur clusters

In the respiratory chain in mitochondrial inner membrane and bacterial cytoplasmic membrane, iron–sulfur clusters exist in three basic structures $[2Fe–2S]^{(2+, 1+)}$, $[4Fe–4S]^{(2+, 1+)}$ [2–4], and $[3Fe–4S]^{(1+, 0)}$ [26]. In Complex I, only the first two forms are encountered. A binuclear cluster is composed of two iron atoms which are bridged by two acid-labile inorganic sulfides, and ligated to four cysteinyl sulfur from polypeptide chain of the apoprotein. Each iron is tetrahedrally coordinated to two acid labile sulfur and two systeinyl sulfur. They function as one electron redox couples, diamagnetic in the oxidized state and paramagnetic in the reduced state at low temperature [27]. In the oxidized state, two high spin ferric iron atoms ($S = 5/2$) are anti-ferromagnetically coupled giving rise to $S = 0$ ground state, accounting for the observed low temperature diamagnetism. In the reduced state, the anti-ferromagnetic coupling between high spin ferric ($S = 5/2$) and high spin ferrous iron ($S = 2$) produces $S = 1/2$ ground state. This spin $1/2$ system exhibits a unique EPR spectrum in which at least two g values are smaller than $g = 2.0023$ (the value for free electron) known as the so called '$g = 1.94$' type signals. This peculiar EPR spectrum was successfully explained by the anti-ferromagnetic spin coupling model by Gibson et al. [28]. The valence electrons in the reduced binuclear [2Fe–

2S]$^{1+}$ cluster are mostly localized at the Fe(II) site. A tetranuclear cluster contains four iron atoms and four acid-labile sulfides arranged in a distorted cube structure with the iron atoms bound to the polypeptide chain via four cysteine sulfur ligands. Four iron atoms can have formal valences of (3, 3, 3, 2), (3, 3, 2, 2), and (3, 2, 2, 2). Under physiological conditions, tetranuclear clusters in Complex I function only in the latter two redox states [they are distinguished as ferredoxin (Fd)-type from the high potential iron–sulfur protein (Hipip)-type clusters which function in the former two redox states], working as single electron carriers. The Fd-type tetranuclear clusters are diamagnetic in the oxidized state and paramagnetic in the reduced state at low temperatures and also exhibit the '$g = 1.94$' type EPR spectra. Therefore, an assumption was made similar to the case of the binuclear spin-coupling model. In the oxidized state two ferric and two ferrous atoms are anti-ferromagnetically coupled, giving effective total spin of $S = 0$, and in the reduced state one ferric and three ferrous iron atoms giving effective total spins of $S = 1/2$ in the cryogenic temperature range. Four iron atoms in the reduced Fd-type tetranuclear clusters were indistinguishable in Mössbauer analysis [29], and it has been considered that the valence electrons are far more delocalized than that of the binuclear cluster. The ^{1}H-NMR, however, could detect a pair-wise localization of valence electrons in the Fd-type [4Fe–4S] cluster in the higher temperature range [30]. Tetranuclear clusters in the oxidized and reduced states have net charge of [4Fe–4S]$^{2+}$ and [4Fe–4S]$^{1+}$, respectively. The spin relaxation of the 3d electrons in the [2Fe–2S]$^{1+}$ clusters is much slower than in the [4Fe–4S]$^{1+}$ cluster, allowing their EPR signals to be detected even at liquid nitrogen temperature (77 K) under the condition where the EPR spectra of the tetranuclear clusters are too broad to be detected. At low temperatures (< 20 K) we can selectively record EPR spectra of tetranuclear clusters, when signals from the binuclear clusters are mostly power-saturated (see Appendix A for more details).

In the early 1970's, the first EPR analyses at temperatures below 77 K were conducted in order to scrutinize the involvement of iron–sulfur clusters in energy coupling in the Complex I segment of the respiratory chain between different yeast strains, i.e., *Candida utilits* versus *Saccharomyces cerevisiae*; the former yeast contains energy transducing Complex I while the latter does not [31,32]. EPR signals from previously unrecognized iron–sulfur clusters were discovered in the former strain. This endeavor led to the spectral resolution of six distinct iron–sulfur clusters, namely, clusters N1a, N1b, N2, N3, N4 and N5 (according to the Ohnishi's nomenclature), which were found to be associated with Complex I. Three laboratories contributed to these results using reductive titrations [33], potentiometric titrations [34] and spectral computer simulations [35].

Using isolated bovine heart Complex I, Beinert's group partially resolved EPR spectra arising from four iron–sulfur clusters which they designated as clusters 1 to 4. Cluster 1, a binuclear cluster ($g_{z,y,x} = 2.022, 1.938, 1.923$) was discovered by Beinert and Sands at 77 K in 1960 [36]. Cluster 2 was defined as the iron–sulfur cluster showing the axial-type spectrum ($g_z = 2.054$ and $g_{x=y} = 1.922$) which was well resolved in reductive titrations at temperatures < 20 K. EPR signals from clusters 3 and 4 were not resolved ($g_z = 2.100$ and $g_x = 1.886$ and 1.862 for clusters 3 + 4) by these experiments, however, Ohnishi subsequently distinguished N3 and N4 signals potentiometrically in pigeon heart submitochondrial particles (SMP) where they exhibited different $E_{m7.2}$ values (-240 and -410 mV, respectively) [34]. Cluster N3 was assigned as $g_{z,y,x} = 2.10$, $\sim 1.93, 1.87$ species and cluster N4 as $g_{z,y,x} = 2.11$, $\sim 1.93, 1.88$ species. Then, Albracht in 1977 proposed a correction of the g_z value of the cluster N3 to 2.037 based on the computer fit for equi-spin content of clusters N3 and N4 from the bovine heart Complex I [35]. Ohnishi experimentally confirmed this finding and revised the g value of cluster N3 in pigeon heart SMP to $g_{z,y,x} = 2.04, 1.93, 1.87$. Albracht designated the cluster N3 as cluster 4 and cluster N4 as cluster 3. This confusion in the nomenclature of these clusters still exists. Additional signals designated arising from cluster N5 ($g_{z,y,x} = 2.07$, 1.93, 1.90) were detected later at a much lower temperature range (< 7 K). Unfortunately there are no comprehensive rules for the nomenclature of these clusters, however, an order was found in the Ohnishi nomenclature, i.e., spin relaxation rates increase in the order of N1 < N5 (the higher the cluster number, the lower the optimal EPR sample temperature as seen in Fig. 2). EPR spectra from two binuclear
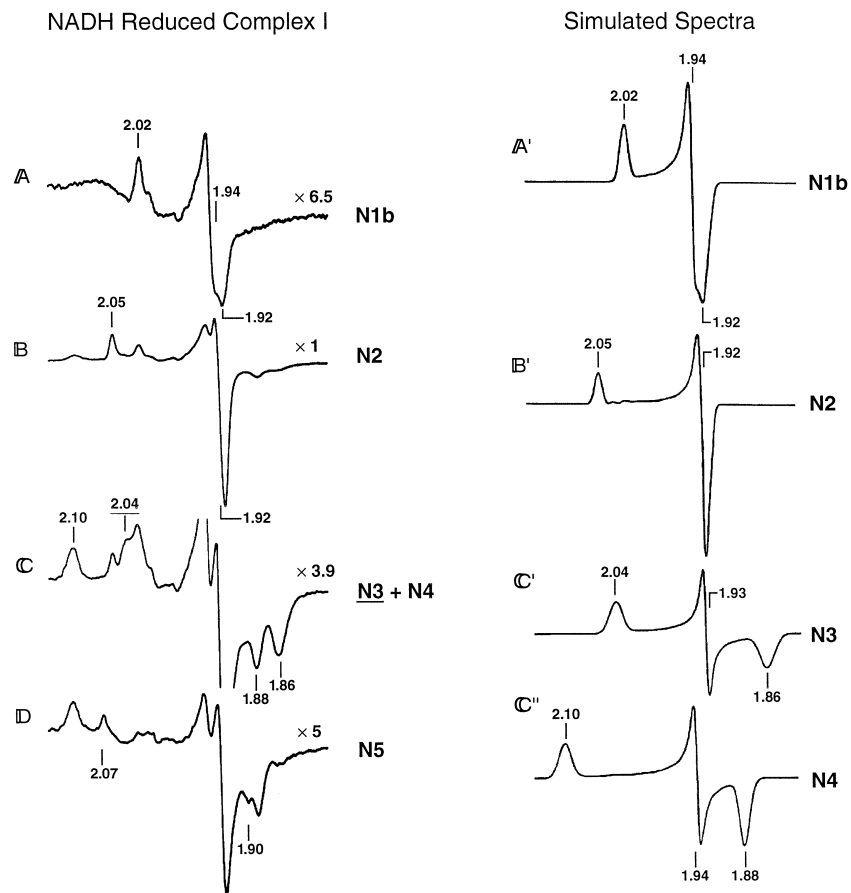
Fig. 2. EPR spectra of iron–sulfur clusters in the isolated bovine heart Complex I reduced by 2 mM NADH. Spectra of iron–sulfur clusters were partially resolved by measuring the same specimen at different temperatures. The sample temperatures were: A, 40 K; B, 12 K; C 9 K; D 7 K. EPR operating conditions are as follows: modulation amplitude, 1.25 mT; microwave power, 5 mW. Computer simulated individual spectra of clusters N1b, N2, N3, and N4 were shown in the right column. Following simulation parameters were used: N1b, $g_{z,y,x} = 2.02, 1.937, 1.922, L_{z,y,x} = 0.88, 0.81, 1.14$ (line width in mT); N2, $g_{z,y,x} = 2.05, 1.924, 1.917, L_{z,y,x} = 0.84, 0.94, 0.88$; N3, $g_{z,y,x} = 2.034, 1.926, 1.858, L_{z,y,x} = 1.50, 0.70, 1.70$; N4, $g_{z,y,x} = 4.099, 1.936, 1.881, L_{z,y,x} = 1.45, 0.80, 1.20$.

clusters were resolved potentiometrically and were distinguished as N1a and N1b. N1a has a $E_{m7.2}$ value of -380 ± 20 mV in SMP, while N1b has a $E_{m7.2} = -240 \pm 20$ mV similar to other members of the isopotential group. To date, two [2Fe–2S] clusters (N1a and N1b) and four [4Fe–4S] clusters (N2, N3, N4 and N5) have been characterized (see Fig. 1).

Spin concentrations of N1b, N2, N3, and N4 are equivalent to the FMN concentration in bovine heart Complex I, while cluster N5 concentration is only about 0.25 to one FMN. As pointed out in my previous mini-review [37], cluster N5 may have an equivalent spin concentration with that of FMN, but 75% of the N5 spins are EPR non-detectable because they may be in the $S = 3/2$ ground state [38,39].

This cluster may exhibit EPR signals near the $g = 5$ region requiring a much higher spin concentration of Complex I (> 0.3 mM) for its clear detection. Cluster N1a is EPR non-detectable in Complex I from different sources, because it remains in the oxidized (diamagnetic) state due to its very low redox midpoint potential (E_m). Thus, only clusters N1b, N2, N3, and N4 were treated as intrinsic Complex I components, but in my opinion, other two clusters (N1a and N5) also remain as intrinsic redox components of Complex I.

An important clue about the total predicted number of iron–sulfur clusters in the Complex I and their possible subunit locations has come from the fully conserved sequence motifs [11,13–15] found on vari-

Table 1

SUBUNIT (*E.coli/ P.denitrificans/* Bovine heart)	CONSERVED MOTIFS AND BINDING SITES.
NuoF/NQO1/51kDa	-CxxCxxC--$(x)_{39}$--C [4Fe-4S]$_{N3}$, NADH and FMN binding sites
NuoE/NQO2/24kDa	-CxxxxC--$(x)_{35}$—CxxxC-, [2Fe-2S]$_{N1a}$
NuoG/NQO3/75kDa	-D-$(x)_6$-E-$(x)_{19}$-C-$(x)_{10}$-CxxC-$(x)_{11-13}$-C-$(x)_{35}$-CxxCxxxxxC-
	$(x)_{38}$-CxxCxxZ-$(x)_{43-46}$-CP-, [2Fe-2S]$_{N1b}$, [4Fe-4S]$_{N4}$, [4Fe-4S]$_{N5?}$
NuoD/NQO4/49kDa, NuoC/NQO5/30kDa	-
NuoB/NQO6/PSST	-CCxxE--$(x)_{60}$--C--$(x)_{30}$—CP [4Fe-4S]$_{N2?}$
NuoI/NQO9/TYKY	-CxxCxxCxxxCP--$(x)_{27-28}$—CxxCxxCxxxCP- two [4Fe-4S]$_{N2?}$
NuoH/NQO8/ND-1	Quinone and rotenone binding site(s)
NuoN/NQO14/ND-2, NuoA/NQO7/ND-3	-
NuoM/NQO13/ND-4, NuoK/NQO11/ND4L	-
NuoL/NQO12/ND-5, NuoJ/NQO10/ND-6	-

The nomenclature of (NuoA–NuoN) was primarily used in this mini-review for Complex I subunits, because it reflects the order of the gene on the *nuo* locus. However, other subunit nomenclatures are also well-used in the literature. Therefore, the conversion table for subunit nomenclature is attached to this table.

ous subunits, which allows for the possibility of up to eight iron–sulfur clusters associated with Complex I (Table 1). Since we have detected only six distinct clusters, the other two tetranuclear clusters have been so far not detected by EPR.

Fig. 2 provides an example of the spectral resolution of EPR signals from individual iron–sulfur clusters, from bovine heart Complex I reduced with NADH. The entire range of iron–sulfur signals arising from all the clusters are observed within a narrow magnetic field (< 50 mT), recorded at different temperatures. Spectra only from the binuclear clusters can be recorded at a higher temperatures range. At 40 K, only a rhombic spectrum of cluster N1b ($g_{z,y,x} = 2.02, 1.94, 1.92$) is observed (spectrum A). At 12 K, an axial-type spectrum of the tetranuclear [4Fe–4S] cluster N2 ($g_{//,\perp} = 2.05, 1.92$) is predominant (spectrum B). This cluster exhibits the slowest spin relaxation among tetranuclear clusters in Complex I. At this temperature (12 K), N1b signals are mostly power-saturated. At 9 K, signals from [4Fe–4S] clusters N3 ($g_{z,y,x} = 2.04, 1.93, 1.87$) and N4 ($g_{z,y,x} = 2.10, 1.94, 1.89$) are more pronounced (spectrum C). At this temperature N2 signals are considerably saturated. In spectrum D recorded at 7 K, signals arising

from the fastest relaxing [4Fe–4S] cluster N5 ($g_{z,y,x} = 2.07, 1.93, 1.90$) are observed together with partially saturated N4 signals. The cluster N3 signals are almost completely saturated at this temperature showing a slower spin relaxation time than that of the cluster N4. Signals from the cluster N1a are not seen in this figure because its E_m value is further lowered in the isolated bovine heart Complex I than in the in situ membrane system. The E_m values of all iron–sulfur clusters and flavin in the Complex I segment of the respiratory chain of the bovine heart SMP are presented in Fig. 1.

2.1. Recent studies using bacterial Complex I

Bacterial Complex I has attracted many researchers' interests because of its relative structural simplicity and the use of genetic tools to manipulate protein [40]. In situ studies of iron–sulfur clusters in the *P. denitrificans*, *R. capsulatus*, and *R. sphaeroides* cytoplasmic membranes showed very similar EPR spectra with the counterpart of the bovine heart Complex I system. However, the isolation of intact Complex I from these bacteria was found to be
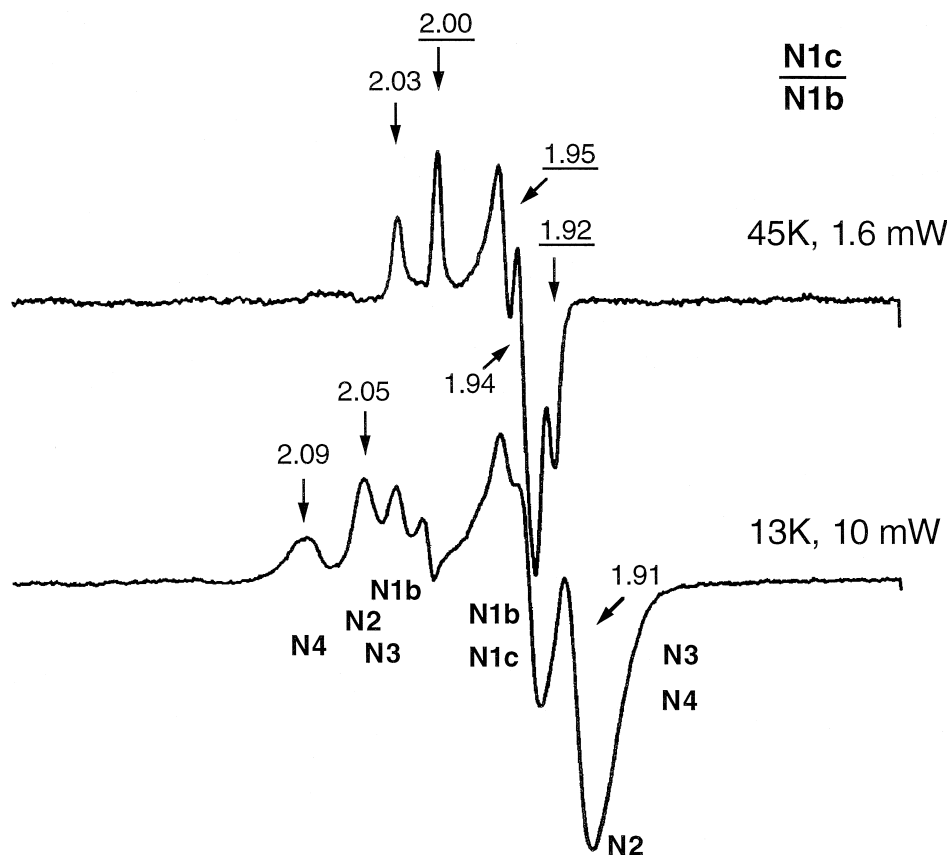
Fig. 3. EPR spectra of the isolated *E. coli* Complex I, recorded under two different EPR conditions as shown. Complex I (8.8 μM) in 50 mM Mes/NaOH (pH 7.2), 50 mM NaCl, 15% sucrose, and 0.4% APG225, was reduced with 2 mM NADH.

much harder to achieve than that of mitochondrial Complex I because of instability after detergent solubilization [17,41,42]. A happy surprise came to the field when Weidner et al. succeeded in the isolation of *E. coli* Complex I, retaining all 14 subunits, subsequent to their cloning and sequencing of the *nuo* operon [13]. Two (C and D) of these subunits were found fused in *E.coli* yielding a 13 subunit enzyme [16]. To date, *E. coli* Complex I is the only bacterial system, which has been studied in all three levels of the structural organization, i.e., in cytoplasmic membrane, in isolated whole Complex I, and in the three defined subfractions, namely, hydrophilic NADH dehydrogenase fragment (NDF), amphipathic connecting fragment, and membrane fragment [43].

In the cytoplasmic membranes of *E. coli* B wild-type strain, EPR spectra of three distinct binuclear (N1a, N1b, and N1c) and three tetranuclear (N2, N3, and N4) clusters have been resolved by combined application of cryogenic EPR and potentiometric titration [43]. EPR spectra of isolated *E. coli* complex I are shown in Fig. 3. The Complex I was reduced with 2 mM NADH, and spectra were recorded at two different temperatures. At 45 K, EPR spectra of binuclear N1b ($g_{//,\perp} = 2.03$, 1.94) and N1c ($g_{z,y,x} = 2.00$, $\underline{1.95}$, $\underline{1.92}$) clusters were observed with axial and rhombic symmetry, respectively. Cluster N1c may arise from the NuoG subunit of *E. coli*. This subunit carries an extra cysteine-motif (C_{228}XXCX-XXC(X)$_{(27)}$C) which is not found in Complex I from mammalian sources [11] or in *P. denitrificans* [20]. This extra cysteine-motif may be related to cluster N1c, because the N1c signals were not observed in the membrane systems which lack this sequence motif. Cluster N1c belongs to the isopotential group as seen in Fig. 1. Cluster N1a was also not reduced by NADH because its E_m value is lower in the isolated complex than seen in the membrane. At 13 K, EPR

signals from the two tetranuclear clusters N2 and N4 have clearly resolved g_z peaks while the g_x feature of all tetranuclear clusters of *E. coli* Complex I are more overlapped than those in the mitochondrial counterparts (cf. Fig. 2). The g_z signal of cluster N3 overlaps with those of N2 and partially saturated N1b.

Using computer simulation, the relative spin concentration of each individual iron–sulfur cluster was approximated and found to be equivalent to that of flavin, namely FMN/N1b/N1c/N2/N3/N4 = 1.0/1.1/1.2/1.0/0.9/1.1 [43]. The FMN content in the isolated complex is 0.9 mol/Complex I (i.e., approximately one to one ratio per Complex I molecule).

As compared with its mitochondrial counterpart, *E. coli* Complex I is more labile, but this feature of the bacterial Complex I has provided an advantage by allowing its Complex I to be cleaved into three subfractions using a relatively mild treatment (changing a detergent from 0.4% alkylglucoside APG225 to 0.3% Triton-X 100 and changing pH from 6.0 to 7.5). The three fractions consist of: the hydrophilic NADH dehydrogenase fragment (NDF, containing the NuoE, F, and G subunits), the amphipathic connecting fragment (containing the NuoB, CD, and I subunits), and the extremely hydrophobic membrane fragment (containing the NuoA, H, J, K, L, M and N subunits, that are equivalent to the mitochondrial gene encoded subunits). The NDF is obtained in a water-soluble form and is easily purified. This fragment contains the NADH and FMN binding sites and transfers electrons from NADH to various artificial electron acceptors, such as ferricyanide and Q_2, via a piericidin A insensitive pathway. The NADH-reduced NDF exhibits EPR spectra arising from clusters N1b, N1c, N3, and N4.

The connecting fragment is not soluble in the absence of a detergent. It exhibits one cluster N2-type EPR spectrum, although the conserved cysteine-rich sequence motifs predict the presence of up to three tetranuclear iron–sulfur clusters between the NuoB (NQO6/PSST) and NuoI (NQO9/TYKY) subunits. Cluster N2 is missing in NDF, and present in the connecting fragment. These observations showed that cluster N2 resides in either the NuoB or the NuoI subunit as suggested by the amino acid sequence motif. No iron–sulfur clusters are present in the

membrane fragment, in agreement with the primary sequence information [43].

2.2. Location of redox centers in individual hydrophilic subunits

Identification of the subunit location of individual redox centers has been conducted by the gene disruption method in the *N. crassa* system [44] and by the analysis of isolated individual *P. denitrificans* subunits expressed in *E. coli* cells and isolated from them by Yano et al. [45].

The NuoE (NQO2) subunit contains one EPR detectable [2Fe–2S] cluster. Because of a partial EPR lineshape modification of the signal compared to intact Complex I (g_z shift 2.03 → 2.00), this cluster could not be unambiguously assigned to N1a or N1b [45] by the EPR method. Previously, we assigned this binuclear cluster as N1b in the 24 kDa subunit of the flavo-iron–sulfur subfraction (called FP) of the bovine heart Complex I resolved by a chaotropic reagent [46,47]. This assignment was based heavily on the fact that this iron–sulfur cluster was reducible with NADH in the FP fraction [45]. However, as described below, N1b was more clearly assigned to the [2Fe–2S] cluster in the NuoG (NQO3/75 kDa) subunit. Since *P. denitrificans* Complex I contains only two binuclear clusters, the [2Fe–2S] cluster in the NuoE (NQO2/24 kDa) subunit was reassigned as the remaining cluster N1a [48]. NuoE (NQO2) subunit contains four conserved cysteine residues arranged in a non-typical cysteine-rich motif as well as three non-conserved cysteine residues and one conserved histidine residue. Using site-directed mutagenesis, the four conserved cysteines were assigned as the ligands of the binuclear iron–sulfur cluster, representing a novel ligation motif (–CxxxxC–CxxxC–) for a [2Fe–2S] cluster [49].

Unfortunately, the *P. denitrificans* NuoF (NQO1/51 kDa) hydrophilic subunit could not be expressed in *E. coli* as a single soluble subunit, because it formed insoluble inclusion bodies. However, this subunit could be co-expressed as a water soluble 1:1 hetero-dimer complex together with the NuoE (NQO2) subunit [50]. The expressed complex, as isolated, contained one assembled [2Fe–2S] cluster residing in NuoE (NQO2), but contained almost no FMN nor [4Fe–4S] cluster. The latter two prosthetic

groups could be partially reconstituted with FMN, Na_2S, and $(NH_4)_2Fe(II)(SO_4)_2$ in vitro. The reconstituted dimer-complex showed EPR signals consisting of two distinct species of iron–sulfur clusters, namely, N1a ($g_{z,y,x} = 2.00, 1.95, 1.92$) and a fast relaxing tetranuclear-type signal with $g_{z,y,x} = 2.04, 1.94, 1.87$. The latter signal is reminiscent of the cluster N3 in the intact Complex I. FMN and cluster N3 were reconstituted independently. Electron transfer from NADH to various electron acceptors was restored in proportion to the amount of FMN reconstituted to the apoprotein, which experimentally demonstrated direct electron and proton transfer from NADH to flavin [50]. Unfortunately in this overexpressed subunit system, both iron–sulfur clusters had considerably lowered E_m values (< -450 mV), thus neither clusters were reducible with NADH.

The *P. denitrificans* NuoG (NQO3/75 kDa) contains 12 conserved cysteines, and one each of aspartate and glutamate residue in the N-terminal region (*T. thermophilus* subunit has only 11 conserved cysteines; the first cysteine in the N-terminal side is not conserved in this thermophile [15]). This distribution predicts the existence of at least three iron–sulfur clusters, and one of them should exhibit an atypical ligand structure. The *P. denitrificans* NuoG (NQO3) subunit was overexpressed in *E. coli* cells and isolated from the cytoplasmic phase. EPR signals arising from one [2Fe–2S] and one [4Fe–4S] cluster were detected in this subunit (0.8 spins each per subunit) based on their different spin relaxation behaviors [48]. The axial type spectrum of the binuclear center with $g_{//,\perp} = 2.026, 1.934$ (linewidth $L_{//,\perp} = 3.0, 1.8$ mT) was very similar to the spectrum of cluster N1b in situ. The EPR spectrum of the tetranuclear cluster was similar to that of cluster N4 ($g_{z,y,x} = 2.063, 1.928, 1.892$; $L_{z,y,x} = 1.75, 1.55, 2.40$ mT) with only a small shift of the g_z value ($2.09 \rightarrow 2.06$). The [4Fe–4S] cluster was very sensitive to oxidants and is readily converted to a [3Fe–4S] cluster, a phenomenon not seen in the intact complex I. Perhaps this cluster is more exposed to the solvent in the isolated subunit than in situ. This purified NuoG subunit contains 8 mols Fe and 9 mol S* per subunit, which is more than needed for one binuclear and one tetranuclear clusters. Localization of a third tetranuclear iron–sulfur cluster was also suggested because a small $g = 5$ EPR signal was detected [48] (Yano et

al., unpublished data). The third cluster could be ligated with mixed cysteine and non-cysteine ligands. This cluster may correspond to the cluster N5, which belongs to the isopotential group ($E_m = -250$ mV) of the iron–sulfur proteins in Complex I [2].

3. Subunit location of cluster N2 and its possible ligand residues

Cluster N2 has been considered to play an important role in the energy conversion in Complex I, since this cluster has the following unique properties: (1) it has the highest E_m value among all iron–sulfur clusters in Complex I, and its E_m value is variable among different membrane preparations [2,51]; (2) its one electron reduction or oxidation is coupled with binding and release of one proton in the physiological pH range [2,51,52]. In other words, its E_m is pH dependent (-60 mV/pH) within the physiological pH range ($6 < pH < 8.5$); 3) its apparent E_m exhibits $\Delta\mu_H^+$ dependence. Although the cluster N2 is not localized in an intrinsic membrane subunit, it is considered to be inserted into the membrane environment, based on the following observations: (i) it cannot be extracted from the membrane without detergents [43,53]: (ii) when bovine heart Complex I was delipidated by 50%, the E_m value of N2 was lowered by 75 mV (while that of all other clusters did not change significantly). The original E_m value was recovered by reconstituting the delipidated sample into liposomes. In parallel, the rotenone sensitive NADH-Q reductase activity was restored [54]; (iii) the disruption of a nuclear-encoded gene for a hydrophobic subunit disturbed the membrane assembly and resulted in the loss of the cluster N2 [44].

The cluster N2 is the only remaining EPR detectable iron–sulfur cluster whose subunit location and the ligand cysteine sequence motif have not been assigned. Our EPR studies on the *E. coli* Complex I subfractions indicated that the cluster N2 is located in the connecting amphipathic subfraction, containing the subunits NuoB, CD, and I. Subunit NuoCD does not contain cysteine motifs for iron–sulfur ligation. Thus, either NuoI or NuoB remains as a candidate for the N2 ligand-containing subunit. The current status of the efforts to determine the location of cluster N2 will be discussed below.

3.1. Considerations from EPR spectral properties and E_m values of iron–sulfur clusters

The NuoI (NQO9) subunit contains stereotypical sequence motifs for ligation of two [4Fe–4S] clusters, similar to the 8Fe-ferredoxin which is considered to be evolutionarily the most primordial structure [55]. In contrast, NuoB contains a primary sequence for possible ligation of one atypical tetranuclear iron–sulfur cluster which is also conserved among primitive iron–sulfur proteins in hydrogenases [56,57]. It was found very difficult to overexpress and purify the *P. denitrificans* NuoI (NQO9/TYKY) and NuoB (NQO6/PSST) subunits, since these subunits readily formed inclusion bodies. However, the NuoI subunit has recently been overexpressed in, and purified from *E. coli*, in a relatively native form (Yano et al., unpublished data), by co-expressing it with *E. coli* thioredoxin [58].

The iron–sulfur clusters were chemically reconstituted in vitro with a reconstitution efficiency of about 30% as judged by the chemically determined non-heme iron content. Our preliminary EPR experiments clearly show EPR signals from two [4Fe–4S] clusters (Fig. 4) with multiple signals at 2.08, 2.05, 1.94, 1.93, 1.90, and 1.88. The 2.01 signal appears to arise
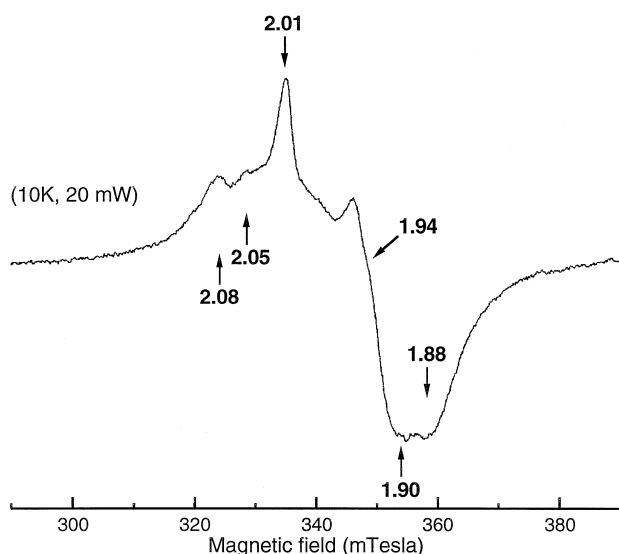

Fig. 4. EPR spectrum of *P. denitrificans* NQO9 (NuoI) subunit, containing stereotypical 2[4Fe–4S] ligation motif, which was overexpressed in *E. coli* cells, purified and chemically reconstituted with Na_2S, $(NH_4)_2Fe(SO_4)_2$, and dithiothreitol in vitro under anaerobic conditions.

from a $[3Fe–4S]^{1+(1+,\,0)}$ cluster which was produced presumably by a modification of a small portion of the original $[4Fe–4S]^{1+(2+,1+)}$ cluster by contact with air oxygen, but its relative spin concentration is very low (Yano et al., unpublished data). This spectral properties is similar to the two analogous [4Fe–4S] clusters, F_A and F_B found in the PsaC subunit of photosystem I (PSI), which contains two stereotypical cysteine sequence motifs for two [4Fe–4S] clusters [59–62]. The X-ray structure of PSI in cyanobacteria is known at 4.0 Å resolution [63]. Spins of the cluster F_A ($g_{z,y,x}$ = 2.04, 1.94, 1.85) and F_B ($g_{z,y,x}$ = 2.06, 1.93, 1.88) are magnetically coupled as seen by slight shifts of their g_z and g_x values [64] and these two clusters show no significant redox interactions [65–67]. Analogous phenomena might be expected in the EPR spectra of the two tetranuclear iron–sulfur clusters which exist in the overexpressed and purified *P. denitrificans* NuoI (NQO9) subunit. When this single protein subunit is overexpressed and purified, the EPR spectra of its iron–sulfur clusters are somewhat modified. However, even taking this modification into consideration, the EPR spectra of NuoI (NQO9/TYKY) in the expressed and purified subunit are quite different from the axial type ($g_{//,\perp}$ = 2.05, 1.92) spectrum of the cluster N2 in situ. When the 'connecting' fragment of *E. coli* complex I is solubilized by detergent treatment, the [4Fe–4S] cluster still maintains an axial-type EPR spectrum similar to that of N2 cluster in situ. These data favor the idea that cluster N2 may not be located in the NuoI (NQO9/TYKY) subunit, but in the NuoB (NQO6/PSST) subunit.

The E_m values of iron–sulfur clusters in the 8Fe-ferredoxin are < -400 mV [68]. F_A and F_B clusters in the PsaC subunit have even lower E_m values; -580 and -520 mV, respectively [69,70]. In contrast, cluster N2 has a much higher E_m value, i.e., $-150 \sim -50$ mV, the highest among all clusters in Complex I.

The NuoB (NQO6) subunit contains four conserved cysteines ($C^{63}C^{64}xxE^{67}$–C^{129}–$C^{158}P$) in the sequence number of *E. coli*. Two adjacent cysteines (C^{63} and C^{64}) cannot function as ligands concurrently, therefore, NuoB possesses only three candidate cysteine ligands with long polypeptide stretches between each. Because the C-terminal end C^{158} is next to a proline, a [4Fe–4S] cluster structure was

suggested. As mentioned earlier, we can expect that if this subunit carries an iron–sulfur cluster, it is likely to have mixed ligand residues where the non-sulfur ligand is the conserved glutamate (E^{67}). In a very preliminary experiment, we observed weak EPR signals at temperatures below 10 K arising from the overexpressed and isolated *P. denitrificans* NQO6 (NuoB/PSST) subunit (Yano et al., unpublished data), which likely contains a [4Fe–4S] cluster. However, further efforts are required to achieve a much higher level of in vivo subunit over-expression and in vitro cluster reconstitution. The involvement of a non-cysteine ligand, either oxygen or nitrogen, in addition to the sulfur ligands, may tend to increase the E_m value than seen in the bacterial ferredoxin-type iron–sulfur clusters with four cysteine ligands. An attractive example would be the Rieske binuclear iron–sulfur cluster of the aerobic respiratory chain which has the E_m of 150–300 mV and EPR spectra with an average g value of 1.91 [71,72]. This cluster was shown to be ligated by two histidine and two cysteine ligands with an average g value of ~ 1.91 [72–74]. On the other hand cluster S1 in Complex II (see Fig. 1) was suggested to have an atypical ligand structure from its conserved sequence motif as well as its $E_{m7.0}$ value in the $-80 \sim +80$ mV range. This [2Fe–2S] cluster shows an average g value of ~ 1.96 similar to normal ferredoxin type iron–sulfur clusters [26,75,76]. Based on the site-directed mutagenesis analysis, a water molecule was suggested as a direct non-sulfur ligand which may be hydrogen bonded to aspartate or cysteine residue [77]. It is likely that a non-cysteine residue is ligated to the Fe^{3+} atom of the binuclear S1 cluster [78]. It should be noted, however, the Rieske cluster in Complex III and the 'Rieske-type' cluster in some dioxygenases (having E_m values of $-150 \sim -50$ mV) show over 300 mV difference in their E_m values, even though both iron–sulfur clusters have the same 2-cysteine and 2-histidine ligands [79,80]. The E_m value is governed only in part by the electronic properties of the metal complex, and multiple factors are known to contribute to the E_m of the iron–sulfur clusters. In addition to the net charge effect of the cluster ligand, hydrogen-bond formation by the nearby backbone amides as well as the access of the amino acid side-chain or solvent dipoles close to the cluster are important contributors [81–83].

It should be noted that several [4Fe–4S] clusters with mixed-ligand systems are known in nature. For example, a hyper-thermophile *Pyrococcus furiosus* [4Fe–4S] ferredoxin is ligated by one aspartate (D) and three cysteine (C) residues with a cluster ligation motif of (CxxDxxC–C). This cluster shows an EPR spectrum with atypical $g_{z,y,x}$ of 2.10, 1.86, 1.80 ($g_{ave.} = 1.92$) detectable at temperatures below 15 K [39]. The D^{14} cluster ligand in *P. furiosus* [4Fe–4S] was identified based on the 1D- and 2D-^{1}H NMR analysis [84]. In this case E_m value of the cluster is as low as four-sulfur ligated ferredoxins. There are cases known that mutation of a sulfur ligand to oxygen or nitrogen-ligand not always increase the E_m value of the cluster [85,86]. On the other hand, the aconitase [4Fe–4S] cluster was shown to be coordinated by three cysteine and one H_2O ligands by the high resolution X-ray structural analysis [87]. The EPR spectrum of the aconitase [4Fe–4S]$^{1+}$ cluster shows the $g_{z,y,x} = 2.07$, 1.95, 1.86 with a $g_{ave.}$ of 1.95 in the absence of the substrate, similar to the usual four-cysteine-ligated iron–sulfur clusters [88]. Here again, these examples suggest that even in the case of the tetranuclear cluster ligated by mixed ligands (sulfur and oxygen or nitrogen), its EPR spectrum can be similar to the all-sulfur ligated cluster [84]. These information suggest localized electron density even in the tetranuclear cluster and provides some support to my very speculative proposal of assigning cluster N2 to the NuoB (NQO6/PSST) subunit and its possible atypical ligand structure.

3.2. Site directed mutagenesis studies to determine the subunit location of cluster N2

Both NuoI (NQO9) and NuoB (NQO6) subunits are strong candidates to harbor the cluster N2. In order to determine the location of cluster N2, great efforts have already been made by two research groups using *R. capsulatus* system (Dupuis' and Albracht's collaborating groups) and *E. coli* system (Friedrich's group). Both groups introduced site-directed mutations into the bacterial chromosome by homologous gene recombination. These two groups, however, have reached contradictory conclusions; the former group has proposed that the cluster N2 resides in the NuoI subunit while the latter group proposed that the cluster N2 exists in the NuoB subunit.

In the *E. coli* system, eight fully conserved cysteine residues (ligand candidates) are located in NuoI, and three ligand candidate cysteines are in the C-terminal region of NuoB. Each cysteine was individually mutated to Ala, one at a time (Ala is similar to Cys in size but never functions as a ligand, contrary to Ser). Mutant *E. coli* cells can grow using the alternative NDH-2 pathway. Because of overlapping intense signals from other non-Complex I redox components, EPR spectra of the mutant Complex I clusters could not be analyzed quantitatively in situ in the membrane. Therefore, EPR spectra were examined on isolated Complex I from individual mutants of NuoI and NuoB. Friedrich et al. (personal communication) obtained EPR spectra of Complex I isolated from two NuoB mutants $C^{64}A$ and $C^{129}A$ ($-CC^{64}xxE-C^{129}-CP-$) and from one NuoI mutant $C^{102}A$ ($-CxxC^{102}xxCxxxCP-$). EPR spectra of the binuclear clusters, which were specifically examined at 40 K, showed no difference from that of the wild-type Complex I in all these three mutants. In contrast, EPR spectra recorded at 13 K clearly showed a lack of the cluster N2 in the two NuoB mutants while N2 was seen in the NuoI mutant. Therefore, Friedrich et al. proposed that the cluster N2 may reside in the NuoB subunit rather than in NuoI [89] (and in this issue).

In the *R. capsulatus* system, there is apparently no NDH-2, but the Dupuis' group found that Complex I mutants can grow under aerobic conditions with lactate as a carbon source [90]. This group analyzed EPR signals of iron–sulfur clusters directly in the chromatophore membrane in situ. They conducted mutagenesis of ligand candidate residues (C → S and C → R) in the NuoI subunit [91]. They found that the mutation of the 4th cysteine in the cluster sequence motif (CxxCxxCxxx**C**P) resulted in no assembly of the Complex I and complete absence of the electron transfer activities. Neither NADH-K_3Fe(CN)$_6$ reductase nor the NADH oxidase activities were detected and no EPR signals from any iron–sulfur clusters in Complex I was observed. Therefore, this mutant could neither prove nor disprove the specific effects of mutation on the ligation of the 4th cysteines. In contrast, the mutation of each of the first three cysteines in ($-$**C**xx**C**xx**C**xxxCP$-$) motifs did not affect the phenotype of the mutants (PS$^+$ and electron transfer activities at the wild-type level only with some variability). According to their interpretation, all iron–sulfur clusters were present in these mutants (based only on the lineshape alteration around the g_y and g_x troughs in the reduced chromatophore), but N2 signals were only partially lost, consistently altering the N1/N2 signal ratio. Thus, they proposed that the two cluster N2 resides in the NuoI subunit and only one N2 was lost by mutation of three cysteines, one at a time (shown above in bold). This group found no phenotype alteration by NuoB mutation (C → S).

Experimentally, both groups are well advanced in genetic strategies, but the apparently conflicting data and conclusions may arise from the complicated nature of the Complex I system. Since 1991, the cluster N2 has been proposed as one of the two [4Fe–4S] clusters in the NuoI (NQO9/TYKY) by Dupuis et al. [92], and more recently Albracht's group assigned

Table 2
Current hypotheses on the subunit location of FMN and iron–sulfur (Fe/S) clusters and the number of subunits in the minimal nuclear-encoded functional unit of bovine heart Complex I

Name of Subunit	Albracht's model [93]		Ohnishi's model (this issue)	
	Prosthetic groups	Number of Subunits	Prosthetic groups	Number of Subunits
NuoG (75 kDa)	1 (N1a), 2 (N4)	1	1 (N1b), 1 (N4), 1 (N5)	1
NuoF (51 kDa)	2 (FMN), 2 (N3)	2	1 (FMN), 1 (N3)	1
NuoE (24 kDa)	1 (N1b)	1	1 (N1a)	1
NuoC (49 kDa)	None	1	None	1
NuoD (30 kDa)	None	1	None	1
NuoI (TYKY)	2 (N2)	1	2 [4Fe-4S]	1
NuoB (PSST)	None or 1[4Fe-4S]	1	1 (N2)	1
Total prosthetic groups: 2 FMN & 8 or 9 Fe/S clusters			1 FMN & 8 Fe/S clusters	

both of the [4Fe–4S] clusters in the NuoI (NQO9/TYKY) subunit as the cluster N2 [93] (see Table 2). Since the C74S mutant Complex I did not assemble, analysis of the mutants of the other three Cys residues is very crucial to draw a final conclusion. In my opinion, more selective and quantitative EPR measurements (at least N1b signals examined at a high temperature and non-overlapping $g_{//}$ signal of N2 cluster below 20 K in the chromatophore) of the individual cluster N1 and N2 spectra may be needed for the analysis of the reduced chromatophore samples of *R. capsulatus* mutants. This is very important since it is known that cluster S1 and S2 signals (which overlap with the g_y and g_x region of the cluster N2 signal) intensify in the Complex I deleted mitochondrial system [25,94]. Negative data on the NuoB mutants also require a more rigorous analysis, since Ser is known to function as a substitute-ligand for the Cys [95]. The *E. coli* mutant data also needs at least one positive control on the mutant of non-ligand Cys. However, putting all of these currently available mutant data together, a speculative interpretation can be developed again that the cluster N2 may reside in the NuoB (NQO6/PSST) subunit rather than the NuoI (NQO9/TYKY) subunit, and this cluster may have a novel arrangement of cluster ligands.

4. Flavin

Complex I contains one non-covalently bound FMN per molecule [25,43,53,96]. It can assume three different redox states, namely, fully oxidized, intermediate semiflavin, and fully reduced state. Based on the potentiometric analysis of the E_m value for the 1st and 2nd electron transfer steps, the stability constant ($K_{stab} = 3.4 \times 10^{-2}$ at pH 7) of the semiflavin which is thermodynamically relatively stable [97] similar to semiflavin of Complex II ($K_{stab} = 2.5 \times 10^{-2}$ at pH 7) [75]. This shows that the flavin in Complex I can function as a converter between a strictly $n = 2$ substrate (NADH) and $n = 1$ electron transfer carriers (iron–sulfur clusters), as seen for various electron-transferring metallo-flavo-enzymes [98]. The flavin in Complex I shows E_m value of -340 mV, which is 133 mV lower than that of free FMN ($E_{m7.0} = -207$ mV), which implies that oxidized form of flavin has four orders magnitude higher affinity to its specific binding site than its fully reduced form. The EPR spectrum of potentiometrically obtained flavin free radical showed an unusually broad line width (2.4 mT), which originates from a strong spin–spin interaction between the semiflavin and cluster N3 [97]. This strong magnetic interaction also results in a large enhancement of the semiflavin spin relaxation as well as a concomitant broadening of the EPR spectrum of cluster N3, extending the earlier indication of the spin-coupling between cluster N3 and semiflavin [3,99].

5. Semiquinones

Early in 1983, Suzuki and King [5] detected semiquinone (SQ) EPR signals in the isolated bovine heart Complex I reduced with NADH. Using Q band EPR (34 GHz), they showed that SQ signals arose from protein bound species by their anisotropic lineshape with $g_{z,y,x} = 2.0060$, 2.0051, 2.0022. They resolved EPR spectra into two distinct species of SQ based on the difference of their power saturation behavior as well as their different sensitivities to rotenone and the sulfhydryl reagent. These SQ signals exhibit extremely slow relaxation because the $g = 2.00$ spectra were observed at room temperature (23°C). Subsequently, using tightly coupled bovine heart SMP, Vinogradov's group [6,100] discovered an extremely fast relaxing SQ species in the Complex I segment of the respiratory chain. This semiquinone signal was found to be $\Delta\mu_H^+$ dependent and rotenone sensitive. These investigators proposed a possible spin–spin interaction of the SQ with the cluster N2 spins. De Jong and Albracht confirmed these observations, but they reported that SQ formation was $\Delta\mu_H^+$ independent [7]. Subsequently de Jong et. al. recognized a pronounced effect of the membrane energization on the saturation behavior of SQ and g_z line shape of the cluster N2. This group was the first to observe the split signals on both sides of the $g_{//} = 2.05$ peak of the cluster N2 in coupled bovine heart SMP, but they interpreted this phenomenon as a reflection of the energy induced protein conformational change of the Complex I. They also concluded that only single species of SQ was present in Complex I and its spin relaxation was enhanced by the energization
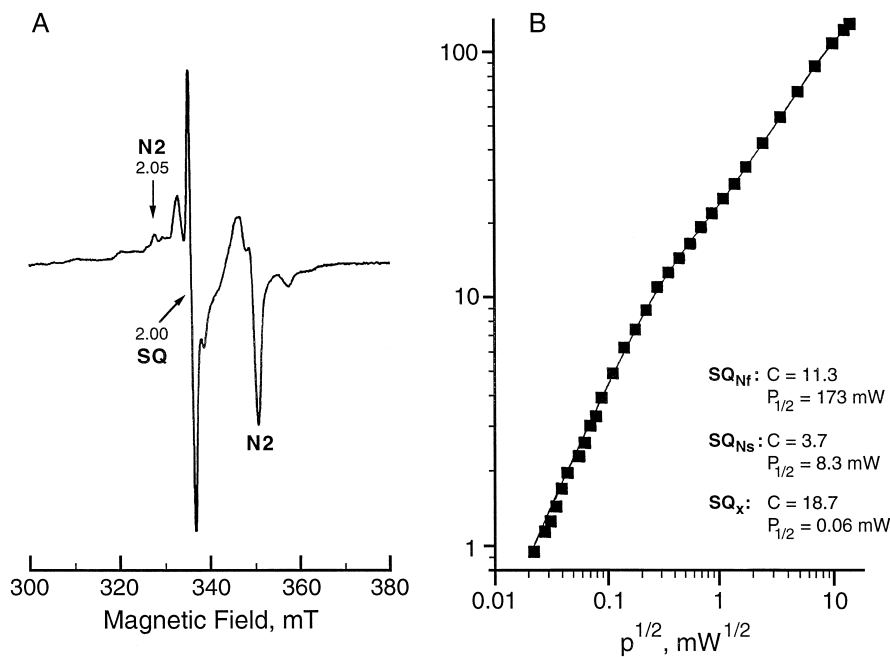
Fig. 5. (A) EPR spectra of tightly coupled (respiratory control RC = 8) activated bovine heart submitochondrial particles during steady-state NADH oxidation. Sample temperature, 16 K, microwave power, 2 mW. (B) Power saturation profile of overlapping semiquinone signals. Sample temperature, 40 K. Power saturation data was analyzed by computer fitting to the equation $A = \Sigma_{i=1}^{n} A_i = \Sigma_{i=1}^{n} C_i \sqrt{P} /(1 + P/P_{1/2(i)})^{0.5b_i}$ where A_i is the amplitude of the i-th type free radical; $P_{1/2i}$ is the half-saturation power and b_i is the homogeneity parameter [102].

[101]. Vinogradov et al. demonstrated the presence of two distinct species of semiquinone in Complex I and designated them as SQ_{Nf} and SQ_{Ns} because of their fast and slow spin relaxation behaviors [102]. They confirmed the splitting of $g_{//} = 2.054$ signal of cluster N2 to $g = 2.044$ and 2.064 peaks and interpreted them to arise from the spin–spin interaction between the cluster N2 and SQ_{Nf}. The dipolar coupling between two spins leads to a broadening or splitting of the signal. Considering the dipolar point approximation, the distance between cluster N2 and SQ_{Nf} can be calculated using the equation $\Delta B = \beta \cdot g \cdot r^{-3} |1 - 3\cos^2\theta|$ where ΔB is the peak separation (in G), r is the distance (in Å) between dissimilar interacting spins, g is the g factor of SQ_{Nf} species, and θ is the angle between the inter-dipolar vector and the magnetic field (H). The distance of 8–11 Å was calculated from the peak-to-peak separation of 3.3 mT. Previously, Salerno et al., demonstrated that the $g_{//}$ direction of the cluster N2 is perpendicular to the membrane, using oriented multilayer preparations [103]. Therefore, if vector connecting SQ_{Nf} and N2

are along the membrane normal, the mutual distance is the longest 11 Å. If the exchange coupling is significant, the distance between cluster N2 and SQ_{Nf} could be as long as 12 Å [102].

The power saturation profile of the $g = 2.00$ SQ signal amplitude is presented in Fig. 5B. In order to visualize multiplicity of the SQ species, a power saturation curve of the $g = 2.00$ signal (at 40 K) was plotted as a function of $P^{1/2}$ in a log–log plot. The tri-phasic power saturation curve was resolved into three individual SQ species, with $P_{1/2}$ values of 173 mW, 8.3 mW, and 0.06 mW, respectively. Based on the enhanced spin relaxation of the SQ_{Nf} by the paramagnetic cluster N2, we obtained a distance (10–13 Å) consistent with that obtained from the splitting (Burbaev et al., unpublished data).

Only the two faster relaxing components of the SQ signals can be quenched by piericidin A at an equivalent concentration to Complex I, leaving one SQ signal with slowest spin-relaxation ($P_{1/2} = 0.06$ mW). Since this is insensitive to the Complex I inhibitors, this may not be associated with Complex I

and it was designated SQ_x. The identity of this SQ species remains to be further examined.

After subtracting this SQ_x signal from the total signal, we can obtain the SQ power saturation curve for the two SQ species associated with Complex I. From this power saturation curve, we also obtained the distance between cluster N2 and SQ_{Nf}. This result was in good agreement with the previous data shown in Fig. 5B (Vinogradov et al., unpublished data).

A weaker magnetic interaction between cluster N2 and SQ_{Ns} is also indicated because the $P_{1/2}$ value of the SQ_{Ns} is clearly higher than a semiquinone species magnetically isolated from other paramagnetic centers. The SQ_{Ns} seems to be further away (~ 30 Å) from the cluster N2, perhaps closer to the cytosolic surface of the membrane. But the accurate distance estimation is difficult to make, because the cluster N2 could extend the spin relaxation effect to SQ_{Ns} via SQ_{Nf}.

Recently, van Belzen et al. reported more detailed experimental data on this topic [104]. They have demonstrated that $g_{//}$ splitting of the cluster N2 indeed arises from magnetic interactions between neighboring spins, because the splitting was found to be independent of the applied microwave frequency (X-band and P-band). Their reported splitting ΔB of 2.8 mT and our 3.3 mT provide almost the same distance r between interacting spins at our resolution level, because the splitting is proportional to r^{-3}. These investigators, however, interpreted that the strong interaction manifested by the $g_{//}$ splitting of the cluster N2 arises from 'exchange coupling' between the two N2 clusters residing within the same subunit, NuoI (NQO9/TYKY). As described in considerable detail in Section 3.2, in my opinion, it is rather unlikely that the two tetranuclear clusters found in the NuoI (NQO9/TYKY) subunit correspond to two N2 clusters. If the disappearance of the $g_{//}$ splitting of the cluster N2 upon addition of the uncoupler is resulted from a protein conformational change of the NuoI subunit (as proposed by Albracht's group), the distance between these two N2 clusters must become longer at least by several angstroms. It is difficult to envision this happening because the 4th cysteines of each [4Fe–4S] cluster binding motif provide the 4th ligand of the other [4Fe–4S] cluster [105] and their cluster assembly is extremely sensitive to a relatively small structural alterations caused

by single site-directed mutagenesis on the 4th cysteine [91,106]. In addition, as discussed earlier in Section 3 the cluster N2 seems to be located in the membrane environment. This is a topic of current intensive work in the Complex I research field.

The data discussed in this section are still at the early stages of investigation and the data interpretation is still controversial, but we favor the idea that the spin–spin interactions observed is primarily between the single cluster N2 and the SQ_{Nf}, and a much weaker interaction between two distinct semiquinone species, namely, SQ_{Nf} and SQ_{Ns}.

6. Conclusion

All the recent work described in this mini-review is summarized in Fig. 6. A hypothetical minimal Complex I model was shaped according to the low resolution L-shape image of *E. coli* Complex I [8,107]. The three subfractions of *E. coli* [43] and the corresponding genes [13] are indicated by gray scale. This drawing places more emphasis on the location of individual redox components, (N1a), (flavin and N3), (N1b, N4, and N5?) in the respective NuoE, F, G subunits, which constitute the hydrophilic NADH dehydrogenase part. In the amphipathic connecting part, the NuoI subunit was found to harbor two [4Fe–4S] clusters analogous to F_A and F_B in the PsaC subunit of PS I. The location of the cluster N2 (NuoB or I) is shown with question marks, because of the conflicting site-directed mutagenesis data, although I favor the NuoB subunit. These two hydrophilic and amphipathic parts form the promontory arm which will constitute a long electron transfer chain connecting the NADH oxidation site and the cluster N2, the latter is located close to the matrix-membrane interface, but inserted into the membrane environment [44,54]. Two distinct species of semiquinone (SQ_{Nf} and SQ_{Ns}) have different spin relaxation behavior; SQ_{Nf} is strongly spin-coupled with cluster N2 (8–11 Å away from each other), while SQ_{Ns} is located closer to the cytosolic side membrane surface and is weakly spin-coupled with cluster N2, perhaps via SQ_{Nf}. We hypothesized the presence of another EPR non-detectable (generating an unstable transition state) semiquinone. It is functionally equivalent to the semiquinone in the Q_o site in Complex III, but acts
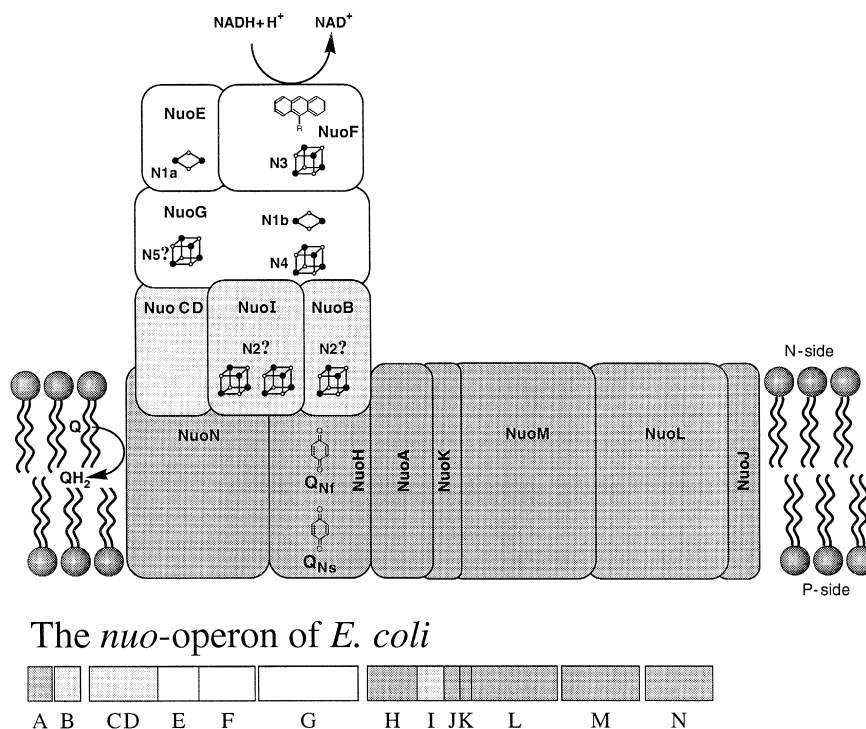
Fig. 6. Schematic outline of the minimal Complex I structure and a summary of our present knowledge on the proposed subunit distribution of different redox centers and Q binding sites. The unusual L-shape image of Complex I is from a low resolution electron microscopic analysis of *N. crassa* Complex I [8,107]. The promontory arm protrudes from the matrix side of the membrane by 80 Å, and the larger hydrophobic arm extends 180 Å within the membrane; analogous long arms were also found in *E. coli* Complex I (Friedrich et al., in this issue). The three subfractions of *E. coli* Complex I and the corresponding genes are indicated in gray scale. The cluster N1c is not included in this figure, because this cluster is not present in the bovine heart, *P. denitrificans*, and *R. capsulatus* Complex I [2,4,40].

as a mirror image of the Q cycle together with the SQ_{Ns} (functionally Q_i site equivalent). SQ_{Nf} was hypothesized to function as an additional proton pumping component to explain the high H^+/e^- stoichiometry in Complex I. A hypothetical model for Complex I energy conversion is proposed in another chapter (Dutton et al., in this issue). These three quinone reaction sites were temporarily placed in the NuoH (ND-1) subunits based on the rotenone analogue binding data [108].

Based on his kinetic data and other information, Albracht and de Jong recently proposed a structural model of complex I [93]. Table 2 compares his model to the model presented in Fig. 6. A basic difference between two models is the flavin content; his proposal of the existence of two flavin-containing subunits per Complex I molecule contradicts the biochemical and immunological assays determining the subunit composition of Complex I from various sources [25,43,53,96]. Several minor differences in

electron transfer mechanisms arise from this two-flavin Complex I model. Exciting and urgent problems concerning Complex I redox components which need to be solved are the controversial issues presented in this mini-review: *the determination of cluster N2 location within the membrane and to define its spatial relationship relative to the distinct quinone binding sites.* This will facilitate the understanding of the mechanism of proton/electron transfer mechanism in Complex I. As evident in the different chapters of this special issue, the field of the Complex I has advanced to the stage that mechanism of this complex enzyme can be clarified using various sophisticated approaches.

Acknowledgements

Appendix A. A brief introduction of EPR technique

The redox components of Complex I are rather poor chromophores for optical spectroscopic analysis in situ both in the mitochondrial and bacterial membranes and even in isolated Complex I. Electron paramagnetic resonance (EPR) spectroscopy has been the most informative technique to detect and resolve signals from individual redox centers. All Complex I iron–sulfur clusters are EPR detectable (paramagnetic) in the reduced state [2–4,109], while flavin and quinone are detectable in the free radical state, i.e., semiflavin or semiquinone state [97,110]. In EPR spectroscopy, only components which have unpaired electrons, such as transition metals or free radicals, are detected.

For simplicity, consider a paramagnetic substance which has free unpaired electrons (spin $S = 1/2$). In the absence of magnetic field, all the spins (illustrated with arrows in Fig. 7) in the samples are oriented randomly at the same energy level. When the sample is placed in a magnetic field (H), the magnetic moment of unpaired spins will tend to be aligned either anti-parallel or parallel to the direction of the magnetic field (called Zeeman splitting). Therefore, spins in the sample are divided into two populations having energies of $-(1/2) g \beta H$ and $+(1/2) g \beta H$. Lower and higher energy levels correspond to spins anti-parallel and parallel to the applied magnetic field, respectively (Fig. 7). In EPR spectroscopy, we observe the resonance transition between these two induced spin populations. The energy difference (ΔE) between these spin states is dependent on the strength of the applied field (H). When microwave with an energy $h\nu$ is applied to this system, and H is scanned, a resonance transition takes place when ΔE between the two states ($g \beta H$) becomes equal to $h\nu$ (h is Planck's constant and β is the Bohr magneton, two fundamental physical constants). This equation to determine the resonance position contains two variables, microwave frequency (ν) and magnetic field (H). EPR spectra are generally obtained by scanning the magnetic field to find the resonance position with
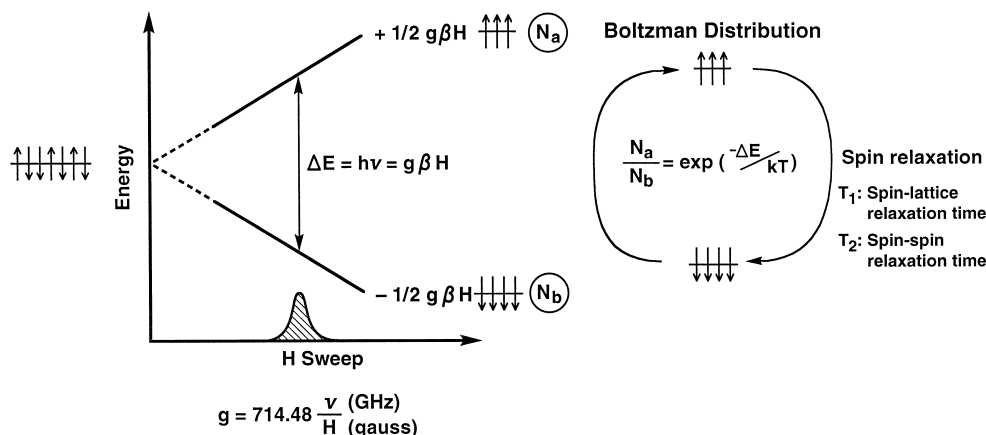

Fig. 7. Schematic presentations of (left) the energy level splitting of unpaired electrons ($S = 1/2$) in an increasing magnetic field, the condition for the electron spin resonance transition, and (right) the Boltzman distribution and spin relaxation phenomena.

a fixed microwave frequency. The most often used frequency is 9 GHz (called X-band). Since EPR detects a very weak energy absorption, modulation of the magnetic field at 100 kHz and phase-sensitive detection are used to increase signal/noise ratio. Therefore, EPR spectra are routinely recorded as the first derivative of the absorption curve.

Since ν varies somewhat from experiment to experiment, it is better to express the signal position in terms of a value characteristic to the substance. In EPR, a g value, which is the constant of magnetization ($g = h\nu/\beta H$), is used to define the position of resonance. For a free electron, g is equal to 2.0023. Since most of the electrons in iron–sulfur clusters are localized in the 3d molecular orbital of transition metal irons, the g value deviates from that of a free electron. This deviation reflects electromagnetic interactions which the spin system has with its surroundings. The g value of a paramagnetic center can have as many as three values, each corresponding to a value obtained when the magnetic field H is parallel to one of the three special directions of the molecule which are called g_x, g_y, and g_z (see Fig. 8). When spins in the molecule are magnetically isotropic, the g value will have a single value ($g_x =$

$g_y = g_z$). In axial or rhombic symmetry, the signal position is given by two ($g_{/\!/}$ and $g_{\perp}$; or in some cases written as $g_{z,y,x}$ with $g_y \cong g_x$) or three (g_z, g_y, g_x) parameters, respectively. Semiflavin and semiquinone show an isotropic $g = 2.005$ spectrum. When g values are close to each other, computer simulation is required to obtain accurate g values. The cluster N2 shows an axial spectrum while N3, N4, and N5 exhibit rhombic spectra in all Complex I so far studied. Cluster N1a and N1b show either axial or rhombic spectra depending on different sources. Since our EPR samples are usually frozen suspensions of submitochondrial particles or enzymes, many molecules of redox components in the EPR samples are randomly oriented. Therefore, the EPR spectra we obtain are summation of signals from redox centers oriented to all directions relative to the magnetic field. They are called polycrystalline powder spectra. The principal g values obtained from powder spectra, as shown in Fig. 8, are approximately equal to the single crystal's principal g values. However relationship between the direction of the crystal axis and these g values must be determined using a single crystal.

The population of spins in the lower energy level (N_B) and higher energy level (N_A) is determined by the Boltzmann distribution [$N_A/N_B = \exp(-g\beta H/kT)$]. The difference between the two populations is generally very small in EPR experiments. When resonance transition occurs, the probability of anti-parallel spin absorbing energy to flip up is equal to the probability of parallel-spins emitting energy to flip down (Fig. 7, Right). Thus, observed net resonance absorption depends on the difference of spin population between the lower and the upper energy states. The spin population in the lower energy level is slightly larger than that of the higher energy level (if both populations are equal, no EPR signal is observed). The applied microwaves tend to equalize these two populations. However, interactions of spins with the molecular environment (called lattice) and interactions between spins themselves tend to maintain the Boltzmann population at a given temperature. This process is called relaxation phenomena. The resonance absorption may be viewed as a continual competition between the tendency of the microwave field to equalize the Boltzmann population difference and the tendency of the spin relax-

SCHEMATIC REPRESENTATION OF THE SHAPE OF THE MAGNETIC MOMENT OF A PARAMAGNETIC CENTER, g VALUES, AND EPR SPECTRAL LINE SHAPE
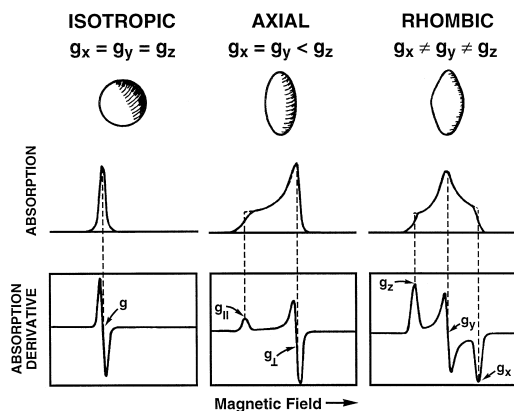

Fig. 8. Schematic presentation of the relationship between g value anisotropy and the EPR spectral line shapes. Geometric shapes of isotropic, axial (prolate form only for our topics), and rhombic magnetic moments are shown as a sphere, a rugby ball, and a rugby ball compressed toward the equator, respectively. Schematic shape of the absorption curves and the corresponding EPR derivative curves are shown in the bottom panels (cited from Ref. [111]).

ations to maintain the difference. The net absorption increases as N_A/N_B becomes smaller (population difference becomes larger) at a lower temperature, as long as the spin relaxation processes predominate.

The relaxation process is characterized by two time constants, T_1 (spin lattice relaxation time) and T_2 (spin–spin relaxation time), both of which are specific properties of the individual paramagnetic components. If the spin relaxation rates ($1/T_1$ and $1/T_2$) are not rapid enough to maintain the population difference during microwave irradiation, the EPR signal intensity decreases. This phenomenon is called power saturation (see Fig. 9). Quantitative analysis of the power saturation behavior of paramagnetic species in the presence and absence of nearby spins is useful for estimating the distance between interacting paramagnetic redox components.

Another important effect of relaxation is related to the spectral line width on the reciprocal of the relaxation time(s) of the paramagnetic species. If the relaxation time(s) are too short, the EPR spectra will be too broad to be detected. For example, EPR signals arising from [4Fe–4S] clusters are known to have extremely short relaxation time(s), and there-

fore, their EPR spectra are detectable only below 20 K.

The amplitude of the derivative spectra (S) is proportional to $P^{1/2}/[1 + 0.25\gamma^2 T_1 T_2 P]^{b/2}$, where γ is the gyromagnetic ratio and factor b is a homogeneous factor; 1 for inhomogeneous (most of the biological samples we study) and 3 for homogeneous power saturation. At a constant temperature, $0.25\gamma^2 T_1 T_2$ is constant, and when P is low and $0.25\gamma^2 T_1 T_2 P < 1$, the signal amplitude ($S$) increases in proportion to $P^{1/2}$. This is the non-power-saturated condition. However, with the application of increased power, S reaches a maximum and then decreases (Fig. 9). The half-saturation parameter $P_{1/2}$ is defined as $4/(\gamma^2 T_1 T_2)$, namely, the shorter the spin relaxation times, the higher the $P_{1/2}$ value becomes. The behavior of the signal amplitude as a function of microwave power is analyzed by measuring the power at the half saturation ($P_{1/2}$) and the degree of homogeneity.

EPR spectroscopy can provide additional useful information on spatial organization by the analysis of EPR spectral changes caused by neighboring magnetically active components. We have applied this technique to determine the distance between intrinsic redox centers and their orientation [3] or the distance between an intrinsic redox center and the surface of the membrane using paramagnetic probe techniques [112,113].

The spin–spin interactions are observed as the enhancement of spin relaxation by more rapidly relaxing spins (Fig. 5B) and/or as the spectral broadening or splitting (Fig. 5A). An excellent example of this approach is the measurement of the remarkable enhancement of semiquinone spin relaxation by the N2 spin. In this system, we could also observe the splitting of the $g_{//}$ of the N2 spectrum by SQ spins, where one can calculate the distance more accurately as explained in section 7 of this mini-review.

An Example of the Homogeneous Power Saturation
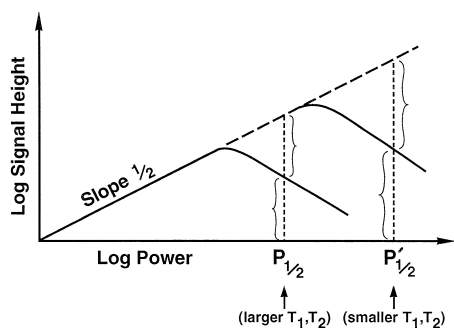
$P_{1/2}$: Power for the Half Saturation with Microwave Energy

Derivative Signal Height $S = A \dfrac{\sqrt{P}}{\left(1+\frac{1}{4}\gamma^2 T_1 T_2 P\right)^{b/2}} = A \dfrac{\sqrt{P}}{\left(1+\frac{P}{P_{1/2}}\right)^{b/2}}$

Half-saturation parameter $P_{1/2} = \dfrac{4}{\gamma^2 T_1 T_2}$ $b = 1$ inhomogeneous
$b = 3$ homogeneous limits

When $P \ll P_{1/2}$ $S = A\sqrt{P}$

Fig. 9. A schematic representation of power-saturation phenomena, definition of the half saturation parameter ($P_{1/2}$), and its relationship with spin relaxation times (T_1 and T_2).

References

[1] N.A. Rao, S.P. Felton, F.M. Huennekens, B. Mackler, J. Biol. Chem. 238 (1963) 449–455.

[2] T. Ohnishi, Membrane Proteins in Energy Transduction, in: R.A. Capaldi (Ed.), Marcel Dekker, New York, 1979, pp. 1–87.

[3] T. Ohnishi, J.C. Salerno, Iron–Sulfur Proteins, Vol. 4, in: T.G. Spiro (Ed.), Wiley, New York, 1982, pp. 285–327.

[4] H. Beinert, S.P. Albracht, Biochim. Biophys. Acta 683 (1982) 245–277.

[5] H. Suzuki, T.E. King, J. Biol. Chem. 258 (1983) 352–358.

[6] D.S. Burbaev, I.A. Moroz, A.B. Kotlyar, V.D. Sled, A.D. Vinogradov, FEBS Lett. 254 (1989) 47–51.

[7] A.M.P. de Jong, S.P.J. Albracht, Eur. J. Biochem. 222 (1994) 975–982.

[8] G. Hofhaus, H. Weiss, K. Leonard, J. Mol. Biol. 221 (1991) 1027–1043.

[9] J.E. Walker, Q. Rev. Biophys. 25 (1992) 253–324.

[10] S.K. Buchanan, J.E. Walker, Biochem. J. 318 (1996) 343–349.

[11] I.M. Fearnley, J.E. Walker, Biochim. Biophys. Acta 1140 (1992) 105–134.

[12] A. Chomyn, M.W.J. Cleeter, C.I. Ragan, M. Riley, R.F. Doolittle, G. Attardi, Science 234 (1986) 614–618.

[13] U. Weidner, S. Geier, A. Ptock, T. Friedrich, H. Leif, H. Weiss, J. Mol. Biol. 233 (1993) 109–122.

[14] T. Yagi, T. Yano, A. Matsuno-Yagi, J. Bioenerg. Biomembr. 25 (1993) 339–345.

[15] T. Yano, S.S. Chu, V.D. Sled', T. Ohnishi, T. Yagi, J. Biol. Chem. 272 (1997) 4201–4211.

[16] F.R. Blattner, G. Plunkett III, C.A. Bloch, N.T. Perna, V. Burland, M. Riley, J. Collado-Vides, J.D. Glasner, C.K. Rode, G.A.F. Mayhew, J. Gregor, N.W. Davis, H.A. Kirkpatrick, M.A. Goeden, D.J. Rose, B. Mau, Y. Shao, Science 277 (1997) 1453–1474.

[17] A. Dupuis, A. Peinnequin, M. Chevallet, J. Lunardi, E. Darrouzet, B. Pierrard, V. Procaccio, J.P. Issartel, Gene 167 (1995) 99–104.

[18] H. Duborjal, A. Dupuis, A. Chapel, S. Kieffer, J. Lunardi, J.P. Issartel, FEBS Lett. 405 (1997) 345–350.

[19] K. Matsushita, T. Ohnishi, H.R. Kaback, Biochemistry 26 (1987) 7732–7737.

[20] T. Yagi, Biochim. Biophys. Acta 1141 (1993) 1–17.

[21] S. Iwata, C. Ostermeier, B. Ludwig, H. Michel, Nature 376 (1995) 660–669.

[22] T. Tsukihara, H. Aoyama, E. Yamashita, T. Tomizaki, H. Yamaguchi, K. Shinzawa-Itoh, R. Nakashima, R. Yaono, S. Yoshikawa, Science 269 (1995) 1069–1074.

[23] T. Tsukihara, H. Aoyama, E. Yamashita, T. Tomizaki, H. Yamaguchi, K. Shinzawa-Itoh, R. Nakashima, R. Yaono, S. Yoshikawa, Science 272 (1996) 1136–1144.

[24] H. Weiss, T. Friedrich, G. Hofhaus, D. Preis, Eur. J. Biochem. 197 (1991) 563–576.

[25] D.C. Wang, S.W. Meinhardt, U. Sackman, H. Weiss, T. Ohnishi, Eur. J. Biochem. 197 (1991) 257–264.

[26] B.A.C. Ackrell, M.K. Johnson, R.P. Gunsalus, G. Cecchini, Chemistry and Biochemistry of Flavoenzymes, Vol. III, in: F. Müller (Ed.), CRC Press, Boca Raton, FL, 1992, pp. 229–297.

[27] G. Palmer, Iron–Sulfur Proteins, Vol. 2, in: W. Lovenberg (Ed.), Academic Press, New York, 1973, pp. 285–325.

[28] J.F. Gibson, D.O. Hall, J.H. Thornley, F.R. Whatley, Proc. Natl. Acad. Sci. U.S.A. 56 (1966) 987–990.

[29] A. Trautwein, Struct. Bonding 78 (1991) 1–95.

[30] I. Bertini, F. Briganti, C. Luchinat, L. Messori, R. Monnanni, A. Scozzafava, G. Vallini, Eur. J. Biochem. 204 (1992) 831–839.

[31] T. Ohnishi, T. Asakura, T. Yonetani, B. Chance, J. Biol. Chem. 246 (1971) 5960–5964.

[32] T. Ohnishi, Biochim. Biophys. Acta 301 (1973) 105–128.

[33] N.R. Orme-Johnson, R.E. Hansen, H. Beinert, J. Biol. Chem. 249 (1974) 1928–1939.

[34] T. Ohnishi, Biochim. Biophys. Acta 387 (1975) 475–490.

[35] S.P. Albracht, G. Dooijewaard, F.J. Leeuwerik, B.V. Swol, Biochim. Biophys. Acta 459 (1977) 300–317.

[36] H. Beinert, R.H. Sands, Biochem. Biophys. Res. Commun. 3 (1960) 41–45.

[37] T. Ohnishi, J. Bioenerg. Biomembr. 25 (1993) 325–330.

[38] L. Yu, I.R. Vassiliev, Y.S. Jung, D.A. Bryant, J.H. Golbeck, J. Biol. Chem. 270 (1995) 28118–28125.

[39] J.B. Park, C.L. Fan, B.M. Hoffman, M.W. Adams, J. Biol. Chem. 266 (1991) 19351–19356.

[40] V.D. Sled, T. Friedrich, H. Leif, H. Weiss, S.W. Meinhardt, Y. Fukumori, M.W. Calhoun, R.B. Gennis, T. Ohnishi, J. Bioenerg. Biomembr. 25 (1993) 347–356.

[41] T. Yagi, Arch. Biochem. Biophys. 250 (1986) 302–311.

[42] S.M. Herter, E. Schiltz, G. Drews, Eur. J. Biochem. 246 (1997) 800–808.

[43] H. Leif, V.D. Sled', T. Ohnishi, H. Weiss, T. Friedrich, Eur. J. Biochem. 230 (1995) 538–548.

[44] W. Fecke, V.D. Sled, T. Ohnishi, H. Weiss, Eur. J. Biochem. 220 (1994) 551–558.

[45] T. Yano, V.D. Sled', T. Ohnishi, T. Yagi, Biochemistry 33 (1994) 494–499.

[46] T. Ohnishi, H. Blum, Y.M. Galante, Y. Hatefi, J. Biol. Chem. 256 (1981) 9216–9220.

[47] T. Ohnishi, C.I. Ragan, Y. Hatefi, J. Biol. Chem. 260 (1985) 2782–2788.

[48] T. Yano, T. Yagi, V.D. Sled', T. Ohnishi, J. Biol. Chem. 270 (1995) 18264–18270.

[49] T. Yano, V.D. Sled, T. Ohnishi, T. Yano, FEBS Lett. 354 (1994) 160–164.

[50] T. Yano, V.D. Sled, T. Ohnishi, T. Yagi, J. Biol. Chem. 271 (1996) 5907–5913.

[51] W.J. Ingledew, T. Ohnishi, Biochem. J. 186 (1980) 111–117.

[52] U. Brandt, Biochim. Biophys. Acta 1318 (1997) 79–91.

[53] M. Finel, J. Bioenerg. Biomembr. 25 (1993) 357–366.

[54] T. Ohnishi, J.S. Leigh, C.I. Ragan, E. Racker, Biochem. Biophys. Res. Commun. 56 (1974) 775–782.

[55] H. Matsubara, K. Saeki, Adv. Inorg. Chem. 38 (1992) 223–280.

[56] T. Friedrich, H. Weiss, J. Theor. Biol. 178 (1997) 529–540.

[57] A. Volbeda, M.-H. Charon, C. Piras, E.C. Hatchikian, M. Frey, J.C. Fontecilla-Camps, Nature 373 (1995) 580–587.

[58] T. Yasukawa, C. Kanei-Ishii, T. Maekawa, J. Fujimoto, T. Yamamoto, S. Ishii, J. Biol. Chem. 270 (1995) 25328–25331.

[59] P.B. Hoj, I. Svendsen, H.V. Scheller, B.L. Moller, J. Biol. Chem. 262 (1987) 12676–12684.

[60] N. Hayashida, T. Matsubayashi, K. Shinozaki, M. Sugiura, K. Inoue, T. Hiyama, Curr. Genet. 12 (1987) 247–250.

[61] H. Oh-oka, Y. Takahashi, K. Kuriyama, K. Saeki, H. Matsubara, J. Biochem. 103 (1988) 962–968.

[62] P.L. Herman, K. Adiwilaga, J.H. Golbeck, D.P. Weeks, Plant Phys. 104 (1994) 1459–1461.

[63] W.D. Schubert, O. Klukas, N. Krauss, W. Saenger, P. Fromme, H.T. Witt, J. Mol. Biol. 272 (1997) 741–769.

[64] M.C. Evans, S.G. Reeves, R. Cammack, FEBS Lett. 49 (1974) 111–114.

[65] R. Cammack, M.D. Ryan, A.C. Stuart, FEBS Lett. 107 (1979) 422–426.

[66] P. Heathcote, D.L. Williams-Smith, C.K. Sihra, M.C. Evans, Biochim. Biophys. Acta 503 (1978) 333–342.

[67] L. Yu, J. Zhao, W. Lu, D.A. Bryant, J.H. Golbeck, Biochemistry 32 (1993) 8251–8258.

[68] R. Cammack, Adv. Inorg. Chem. 38 (1992) 281–322.

[69] J.H. Golbeck, Biochim. Biophys. Acta 895 (1987) 167–204.

[70] J.H. Golbeck, The Molecular Biology of Cyanobacteria, D.A. Bryant (Ed.), Kluwer Academic Publishers, Amsterdam, the Netherlands, 1994, pp. 319–360.

[71] R.C. Prince, J.G. Lindsay, P.L. Dutton, FEBS Lett. 51 (1975) 108–111.

[72] E. Davidson, T. Ohnishi, E. Atta-Asafo-Adjei, F. Daldal, Biochemistry 31 (1992) 3342–3351.

[73] R.J. Gurbiel, D.E. Robertson, F. Daldal, T. Ohnishi, B.M. Hoffman, Biochemistry 30 (1991) 11579–11584.

[74] R.D. Britt, K. Sauer, M.P. Klein, D.B. Knaff, A. Kriauciunas, C.A. Yu, L. Yu, R. Malkin, Biochemistry 30 (1991) 1892–1901.

[75] L. Hederstedt, T. Ohnishi, Molecular Mechanisms in Bioenergetics, L. Ernster (Ed.), Elsevier, Amsterdam, 1992, pp. 163–198.

[76] C. Hägerhäll, Biochim. Biophys. Acta 1320 (1997) 107–141.

[77] M.T. Werth, G. Cecchini, A. Mandori, B.A.C. Ackrell, I. Schröder, R.P. Gunsalus, M.K. Johnson, Proc. Natl. Acad. Sci. U.S.A. 87 (1990) 8965–8969.

[78] W.E. Blumberg, J. Peisach, Arch. Biochem. Biophys. 162 (1974) 502–512.

[79] U. Liebl, V. Sled, G. Brasseur, T. Ohnishi, F. Daldal, Biochemistry 36 (1997) 11675–11684.

[80] B. Rosche, S. Fetzner, F. Lingens, W. Nitschke, A. Riedel, Biochim. Biophys. Acta 1252 (1995) 177–179.

[81] R. Langen, G.M. Jensen, U. Jacob, P.J. Stephens, A. Warshel, J. Biol. Chem. 267 (1992) 25625–25627.

[82] G.R. Moore, G.W. Pettigrew, N.K. Rogers, Proc. Natl. Acad. Sci. U.S.A. 83 (1986) 4998–49999.

[83] S. Iwata, M. Saynovits, T.A. Link, H. Michel, Structure 4 (1996) 567–579.

[84] L. Calzolai, C.M. Gorst, Z.H. Zhao, Q. Teng, M.W. Adams, G.N. La Mar, Biochemistry 34 (1995) 11373–11384.

[85] A. Agarwal, D. Li, J.A. Cowan, J. Am. Chem. Soc. 118 (1996) 927–928.

[86] G. Brasseur, V. Sled', U. Liebl, T. Ohnishi, F. Daldal, Biochemistry 36 (1997) 11685–11696.

[87] A.H. Robbins, C.D. Stout, Proteins Struct. Funct. Genet. 5 (1989) 289–312.

[88] M.C. Kennedy, L. Mende-Mueller, G.A. Blondin, H. Beinert, Proc. Natl. Acad. Sci. U.S.A. 89 (1992) 11730–11734.

[89] T. Friedrich, M. Braun, V. Spehr, B. Pohlkotte, Biochim. Biophys. Acta 9 (1996) 144.

[90] A. Dupuis, A. Peinnequin, E. Darrouzet, J. Lunardi, FEMS Microbiol. Lett. 148 (1997) 107–114.

[91] M. Chevallet, E. Darouzette, H. Duborjal, A. Dupuis, J. Lunardi, V. Procaccio, V. Belzen, S.P.J. Albracht, J.P. Issartel, Biochim. Biophys. Acta 9 (1996) 142.

[92] A. Dupuis, J.M. Skehel, J.E. Walker, Biochemistry 30 (1991) 2954–2960.

[93] P.J.A. Albracht, A.M.P. de Jong, Biochem. Biophys. Acta 1318 (1997) 92–106.

[94] R.W. Moreadith, M.L. Batshaw, T. Ohnishi, D. Kerr, B. Knox, D. Jackson, R. Hruban, J. Olson, B. Reynafarje, A.L. Lehninger, J. Clin. Invest. 74 (1985) 685–697.

[95] J. Meyer, J. Fujinaga, J. Gaillard, M. Lutz, Biochemistry 33 (1994) 13642–13650.

[96] G. Belogrudov, Y. Hatefi, Biochemistry 33 (1994) 4571–4576.

[97] V.D. Sled, N.I. Rudnitzky, Y. Hatefi, T. Ohnishi, Biochemistry 33 (1994) 10069–10075.

[98] D.E. Edmondson, G. Tollin, Top. Curr. Chem. 108 (1983) 109–138.

[99] J.C. Salerno, T. Ohnishi, J. Lim, W.R. Widger, T.E. King, Biochem. Biophys. Res. Commun. 75 (1977) 618–624.

[100] A.B. Kotlyar, A.D. Vinogradov, Biokhimiia 54 (1989) 9–16.

[101] A.M. de Jong, A.B. Kotlyar, S.P. Albracht, Biochim. Biophys. Acta 1186 (1994) 163–171.

[102] A.D. Vinogradov, V.D. Sled, D.S. Burbaev, V.G. Grivennikova, I.A. Moroz, T. Ohnishi, FEBS Lett. 370 (1995) 83–87.

[103] J.C. Salerno, H. Blum, T. Ohnishi, Biochim. Biophys. Acta 547 (1979) 270–281.

[104] R. van Belzen, A.B. Kotlyar, N. Moon, W.R. Dunham, S.P.J. Albracht, Biochemistry 36 (1997) 886–893.

[105] E.T. Adman, L.C. Sieker, L.H. Jensen, J. Biol. Chem. 251 (1976) 3801–3806.

[106] J.M. Moulis, V. Davasse, M.P. Golinelli, J. Meyer, I. Quinkal, J. Biol. Inorg. Chem. 1 (1996) 2–14.

[107] V. Guénebaut, A. Schlitt, H. Weiss, K.R. Leonard, T. Friedrich, J. Mol. Biol. 276 (1998) 105–112.

[108] F.G.P. Early, S.D. Patel, C.I. Ragan, G. Attardi, FEBS Lett. 219 (1987) 108–113.

[109] M.K. Johnson, Encyclopedia of Inorganic Chemistry, Vol. 4, in: R.B. King (Ed.), Wiley, UK, 1994, pp. 1896–1915.

[110] J.R. Bowyer, T. Ohnishi, Coenzyme Q, in: G. Lenaz (Ed.), Wiley, New York, 1985, pp. 409–432.

[111] G. Palmer, Biochem. Soc. Trans. 13 (1985) 548–560.

[112] H. Blum, J.R. Bowyer, M.A. Cusanovich, A.J. Waring, T. Ohnishi, Biochim. Biophys. Acta 748 (1983) 418–428.

[113] T. Ohnishi, H. Schägger, S.W. Meinhardt, R. LoBrutto, T.A. Link, G. von Jagow, J. Biol. Chem. 262 (1989) 735–744.